(Received 27 September 2023, Accepted 24 November 2023, Scheduled 5 December 2023)

Design of Radiation Protection Topology for Pulsed High Currents in Electromagnetic Launcher Based on Decision Variable Analysis

Heyang Wang[1,2,*], Jian Sun[1,2], Yuantao Cong[1,2], Mingjie Zhong[1,2], and Binyu Zhu[1,2]

[1] *Institute of Electrical Engineering, Chinese Academy of Sciences, Beijing 100190, China*
[2] *University of Chinese Academy of Sciences, Beijing 100094, China*

ABSTRACT: Aiming to address the problem of radiation interference caused by pulse high current in the electromagnetic launcher's working process, this study presents a model for selecting materials for the protection of radiation sources and designing their topological structure. Initially, an analysis is conducted on the selection of materials and topology for the protective characteristics, considering factors such as protective effectiveness, production cost, structural rigidity, reliability, and mobility. Through shielding process, several factors influencing material selection are identified. Subsequently, weights and excitation functions are assigned to these factors to generate an applicability evaluation function of the protective materials, aligning with the test requirements. Next, three structures are defined for the test environment: inner shield, outer shield, and wrap-around shield, in accordance with the established protection topology. Using ANSYS, a three-dimensional simulation model is constructed, featuring a peak pulse current of 281.98 kA and an armature mass of 10 g. The shielding performance of materials with thicknesses of 3 mm, 5 mm, 7 mm, and 10 mm is analyzed. Simulation results demonstrate that the outer shielding structure and wrap-around shielding structure can achieve a magnetic induction strength of less than 0.5 T at approximately 6 mm thickness, validating the feasibility of the proposed model. This paper presents a method for addressing electromagnetic radiation protection from the electromagnetic launcher, ensuring the safety of personnel near the gas pedal and the stable operation of electronic components. The findings have significant implications for the future application of the system.

1. INTRODUCTION

Pulsed high-current sliding electric contact gas pedals offer several advantages over traditional acceleration methods, including low energy cost, high injection velocity, high kinetic energy, and low noise [1–4]. These pedals are commonly used for high-speed impact tests in aerospace, land, ocean, and other fields. Typically, the pulsed high-current gas pedal can accelerate an object to a speed of 2 km/s within 10 ms. However, it requires a pulsed high current with an amplitude of 200 kA–600 kA. The intense magnetic field generated by these high currents and voltages can instantly damage sensitive electronic devices and significantly interfere with the normal functioning of microelectronic components [5–7]. Therefore, it is crucial to investigate methods to enhance the radiation shielding capability and electromagnetic compatibility of the weapon system itself.

As early as the early 1940s, the research on electromagnetic interference problems by a single device shielding research has been gradually developed into a theoretical and technical analysis of the overall protection. In the 1970s, domestic electromagnetic shielding research entered a period of rapid development. In terms of electromagnetic shielding theory, Zhang et al. [8] studied the electromagnetic field characteristics of the electromagnetic pulse process, and the shielding effectiveness of the power supply in the peak $5 \sim 6$ kV, 120 kA extreme environment can reach 41 dB. In terms of structural design and effectiveness analysis, Luo and Mei [9] investigated the use of a positional layout in combination with shielding by flexible magnetically conductive materials to protect the fuzes of electromagnetically driven munitions from strong magnetic fields. Liao and others [10] designed single-layer shield, multilayer combined shield, thickness-added shield, and length-added shield using various conductive materials and calculated and compared the shielding effectiveness. Li [11] analyzed the characteristics of the magnetic field inside the chamber during the launching process of an orbital-type extreme electromagnetic energy device, designed different shielding body schemes, and analyzed their shielding effectiveness. In the design of the shielding structure, Li [11] optimized the design of the shielding structure by analyzing the influence of the shielding material, structure, position, and the shape of the bottom through-hole on the shielding effectiveness. However, most of the above researches were aimed at protection efficiency, without systematic consideration of other aspects such as structural rigidity, reliability, space occupation, mass production, and production cost, and there is still room for the improvement of light weight and high efficiency in terms of structure. This paper combines the theoretical analysis of electromagnetism, material science and topology to design a more optimal material and structure of the protective body on the outer side of the acceleration device.

* Corresponding author: Heyang Wang (w15931186726@163.com).

This paper focuses on the analysis of material selection and topology of the protective body, as well as the selection factors for the shielding process. It establishes a material evaluation function model to evaluate several protective materials. After that, the paper carries out the design of the protective topology from three aspects, namely, the inner side, outer side, and wrap-around type, then simulates the shielding effect of the thicknesses of 3 mm, 5 mm, 7 mm, and 10 mm in the experimental environment. The test results show that the magnetic field strength of the protected area is controlled within 0.1 T at a thickness of 10 mm in the model of this paper, which verifies the feasibility of the protective structure of this paper.

2. THEORETICAL MODEL OF ORBITAL ELECTROMAGNETIC GAS PEDAL

2.1. Theoretical Structure of the Gas Pedal

The mechanism of the orbital type electromagnetic gas pedal is to accelerate the carrier by the electromagnetic force between the magnetic field generated by the orbital current and the current of the carrier. This propulsion method is based on the Lorentz force generated by the electromagnetic field theory, rather than a chemical reaction. The electromagnetic force propels the object, and its speed is directly proportional to the current, allowing for higher speeds. The simplified equation of motion is Equation (1).

$$\begin{cases} F = \vec{B}IL = kI^2 = \frac{1}{2}\left(\frac{dL_r}{dt}\right)I^2 = ma_p \\ v_p = v_0 + \int_0^l a_p dt = v_0 + \frac{1}{2m} \cdot \frac{dL_r}{dx} \cdot \int_0^l I^2 dt \end{cases} \tag{1}$$

In Eq. (1), B is the magnetic magnetic flux denisity, I the guideway current, L the inner width of the guideway, L_r the inductance of the guideway, m the mass of the armature, v_p the speed of the armature, v_0 the initial speed of the armature, x the position of the armature, a_p the transient acceleration of the armature, and t the time.

Combining the inductive energy storage formula and ohmic loss formula, the inductive gradient L' and resistive gradient R' of the two-dimensional surface are given by

$$L' = \frac{1}{I^2}\iint_S \frac{\vec{B}^2}{\mu}\,dS; \quad R' = \frac{1}{I^2}\iint_S \frac{\vec{J}^2}{\sigma}\,dS \tag{2}$$

2.2. Structural Design of Radiation Protection for Gas Pedals

Combined with existing research findings, it is believed that with the use of skinning effect and magnetic bypass theory, we can achieve magnetic field radiation protection in the target area. These conductive materials generate an induced magnetic field in the opposite direction of the source magnetic field, thereby mitigating some of the radiation. Additionally, magnetically conductive materials facilitate the magnetic field to 'flow' through the protective materials with higher permeability, reducing the intensity of the 'flow' through the area of electronic components. This approach aims to minimize the strong electromagnetic interference caused by the compacted structure [12–14].

2.2.1. Shielding Material

The effectiveness of shielding is directly influenced by the properties of the shielding materials. When selecting shielding materials, it is important to consider the electromagnetic properties of the materials as well as the source of electromagnetic interference. Additionally, factors such as corrosion resistance, reliability, structural rigidity, processing precision, and cost should are also taken into account to enhance the reliability and applicability of the shielding [11, 15].

Table 1 presents the relative magnetic permeability to air and other properties of various metallic materials. Among these materials, those with relatively high permeability include iron, steel, hot rolled silicon steel, high magnetic permeability silicon steel, pozzolanic alloys, and ferronickel-aluminum alloys. In terms of magnetic saturation, iron-nickel-molybdenum alloys exhibit high permeability, but they are expensive and not easily produced in large quantities. Therefore, a multi-factor material selection model is necessary to consider multiple factors and establish screening selection rules for choosing optimal protective materials.

2.2.2. Selection Factors of Protection Materials to Pulsed High-Current Conditions

We define the selection factors of protective materials based on five parameters: shielding effectiveness S_{EH}, stiffness F, reliability Re, mobility S_P, and production cost P. Translate the five dimensions into the same space. The higher the score of the evaluation function is, the higher the adaptability and feasibility of the material are, and the selected evaluation factors are defined specifically as follows:

1) Protective efficacy S_{EH}. In this paper, the shielding effectiveness (S_{EH}) uses the definition of shielding attenuation: In the electromagnetic field at the same location without the presence of shielding electromagnetic field strength and shielding after the ratio of electromagnetic field strength.

$$S_{EH} = 20\log_{10}\left|\frac{E_2}{E_1}\right| = 20\log_{10}\left|\frac{H_2}{H_1}\right| \tag{3}$$

In Equation (3), E_2, H_2 are the electric and magnetic field strengths at the measuring surface when the protective body is added, and E_1, H_1 are the electric and magnetic field strengths at the measuring surface when there is no protective body.

2) Stiffness or stress S_T. This paper uses the definition of stress f_N, and the source of the force of the shock wave is the external normal electromagnetic force during the high-speed movement of the armature. Since a device may be set up with multiple guards, let Sq be the contact area between the armature and the track, F_N be the electromagnetic force normal to the outside of the armature, k be the offset coefficient, δ_i be the deformation distance in the direction of the force, δ' and δ'' be the offsets, denote the thickness of the guard among the m guards, and h_i be the excitation function, and the stiffness property of the guard material can be expressed as

$$S_T = \phi\left\{\sum_{i=1}^{m}\left(\frac{F_{Ni}}{(k\cdot e)^{\delta_i}\cdot S_q}\cdot\frac{h_{\min}}{h_i} + \delta_i'\right)\right\} + \delta_i'' \tag{4}$$

TABLE 1. Parameters and properties of selected shielding materials.

Material type	Makings	Relative permeability	Impact Stress Resistance	Physical Properties	Material density	Cost (¥/kg)	Causality
Pure metal	Copper	1.72	200–300 Mpa	Abrasion resistance	8.96 g/cm^3	≈ 68	Common
	Iron	200–400	176–274 MPa	Corrosion resistance	7.86 g/cm^3	≈ 4	Common
Common Alloys	Copper-tin alloy	1.96	667 MPa	High hardness, Malleability, Corrosion resistance	8.5 g/cm^3	≈ 66	Common
	Cast iron	100–750	65.5–1450 MPa	Pressure resistance	5.54–7.81 g/cm^3	≈ 5	Common
	Iron-nickel-molybdenum	2000–50000	/	Rare material	8.75 g/cm^3	≈ 1000	Rarity
	Mumetal Permalloy	12000	530–900 MPa	High Temperature Resistant, High Pressure, Resistant Corrosion resistant	8.80 g/cm^3	≈ 230	Common
Rare Alloys	NdFeB magnets	1.05	41.4 MPa	Unwearable	8.40 g/cm^3	≈ 1000	Rarity
Ferromagnetic metal	Cold-rolled steel	2000–3000	1200–1500 MPa	High temperature, Impact stiffness	7.85 g/cm^3	≈ 3	Common
	Steel1008	1000 ∼ 3000	330 MPa	Impact resistance	7.85 g/cm^3	≈ 10	Common
	Stainless steel	1500	25.0–2500 MPa	Corrosion resistance	7.85 g/cm^3	≈ 10	Common
	High magnetic steel	7000–10000	331 MPa	High permeability	7.65 g/cm^3	≈ 35	Rarity
Nonmetallic ferromagnetic	Ferrite	10–1000	50.0 MPa	Impact resistance	4.80 g/cm^3	≈ 2	Common
	Manganese-zinc ferrite	300–5000	/	Impact resistance	1.5 g/cm^3	/	Common
Synthetic material	Graphene-glass fiber	280	600 Mpa	High hardness, High temperature resistance, Corrosion resistance	1.5–2.0 g/cm^2	≈ 800	Common

3) Dependability R_e. The use of the protective body of the gas pedal is characterized by difficult maintenance and high replacement costs, so the reliability of the material is particularly important for the proper functioning of the equipment.

The rules for evaluating reliability include necessary properties and optimized properties are properties that the material must have, such as the resistance to high temperatures, flame retardancy, and high pressure. Each of the above characteristics is assigned a base value of 1, and the weights ω change with environmental adaptation, then the reliability *Re* can be expressed as

$$R_e = \prod_{i=1}^{n_1} M_i \cdot \sum_{j=1}^{n_2} (\omega_j \cdot C_j) \tag{5}$$

In Eq. (5), n_1 is the number of necessary attributes the material possesses, n_2 the number of optimized attributes, M_i the necessary property to be possessed, $M_i = 1$ when the material is possessed, and $M_i = 0$ if the material does not have the above property. C_j is the optimized characteristic, again $C = 1$ when the material contains the above characteristic, and $C = 0$ if it does not.

4) Mobility S_P. Due to the high mobility requirements of gas pedals, space miniaturization and weight lightening are among the structural design considerations. The cross-section space boundary takes the tangent lines of the left and right structural surfaces of the overall outer side of the guard body as the left and right boundaries with a length of l_1, the planar tangent lines of the upper and lower structural surfaces as the upper and lower boundaries with a length of l_2, and the length of the guard in the direction of armature motion is the same as the length of the track l. Corresponding to the density of the protective material as ρ_i and the weight of the protective body expressed as $M_i = \rho_i \cdot V$, the mobility S_P can be expressed as the product of space and weight

$$\begin{aligned} S_V &= \psi_i \cdot S_P \cdot M_i \\ &= \psi_i \cdot \left(\prod_{i=1}^{2} (l_i + \varepsilon_i) \cdot (l + \varepsilon) + v \right) \cdot \rho_i \cdot V \end{aligned} \tag{6}$$

5) Cost P. Production costs consist of material purchase costs p_1, processing costs p_2, and assembly p_3. The guard is a cylindrical body parallel to the rail, so the volume can be expressed as $V = L \cdot h \cdot k/1000$, where L is the length, h the thickness, and k the height, and all units are in mm. Then the cost of production can be expressed as

$$P = \frac{L \cdot k \cdot h}{1000^3} \cdot m + p_2 + p_3 \tag{7}$$

2.2.3. Evaluation Function for Material Selection

Based on the selection of factors and corresponding weights, and combining the function characteristics to establish the evaluation function Z, the protection body material selection prioritizes the protection effectiveness, followed by stiffness, reliability, occupied space, and production cost. Therefore, the weighting function for protection effectiveness is higher than the other factors to highlight the more important characteristics. This paper aims to evaluate the function based on the definition of the exponential function. The exponential function, which has a domain greater than 0, exhibits monotonically increasing and decreasing characteristics by changing the sign of the exponential. Therefore, this paper evaluates the function based on the definition of the exponential function.

$$\begin{aligned} Z(\xi) &= \exp(\xi_1 \cdot S_{EH}) + \xi_2 \cdot S_T + \xi_3 \cdot R_e \\ &\quad + \exp(-\xi_4 \cdot S_P) + \exp(-\xi_5 \cdot P) \end{aligned} \tag{8}$$

The incentive function aims to optimize the calculation speed of the model and prevent excessive computational costs caused by large or small data. It can be likened to the process of normalizing chemical analysis. The variables of the evaluation function of Eq. (8) are related to the structural design of the protective body, which also takes into account the characteristics of the evaluation factors and optimizes the protective effectiveness as much as possible. The weights are dynamically entered with reference to the actual demand for existing protective materials.

$$\Phi\{\xi_i'\} = \Phi\left\{\sum_{i=1}^{5}(\theta_i \cdot \xi_i) + \delta\right\} \tag{9}$$

In Eq. (9), ξ' is the update weights, θ_i the rotation matrix, and δ the bias constant.

2.3. Topology Optimization of Gas Pedal Radiation Source Shielding Body

The law of electromagnetic induction states that a large current produces a magnetic field around a wire. The distribution of the magnetic field is one of the most important parameters for analyzing electromagnetic radiation, and the steady magnetic field of a homogeneous medium is expressed as

$$\vec{B} = \frac{\mu}{4\pi}\oint_L \frac{Id\vec{l} \times \vec{r}}{r^3} \tag{10}$$

When a pulsed high current is passed inside the gas pedal track, it will be accompanied by an induced vortex field. Let the magnetic field strength be $\vec{H}$, the electrical conductivity be σ, and the magnetic conductivity be μ. The general vortex equation can be expressed as

$$\nabla^2\vec{H} = \sigma\mu\frac{\partial\vec{H}}{\partial t} - \nabla\left(\vec{H}\cdot\frac{1}{\mu}\nabla\mu\right) - \frac{1}{\sigma}(\nabla\sigma)\times\nabla\times\vec{H} \tag{11}$$

The combination of Eq. (10) and Eq. (11) allows for a general description of the distribution pattern of the magnetic field radiation and the placement of protective bodies in areas of dense electromagnetic distribution.

2.3.1. Protective Body Topology

Figure 1 illustrates the topology of the shield, disregarding the subtle articulation gaps between the materials. The topological relationship between the shield and the gas pedal can be simplified into two categories: contact and non-contact. The dashed line in Fig. 1 represents the possibility of two modules coming into contact, while the dashed box indicates an alternate topology change module used in cases of extreme ambient currents exceeding 500 kA or radiation less than 0.5 T after demand shielding.

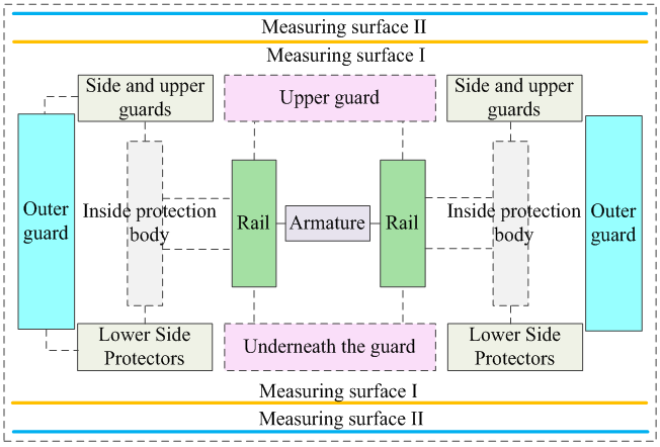

FIGURE 1. Electromagnetic radiation shielding body topology.

2.3.2. Optimization of the Structure of the Protective Body Combination

A shield topology combination is a combination of multiple shields that are fused together to encircle the radiation source as much as possible, thus increasing the protection performance of the space. In this paper, two types of base protection structures, inner connection and outer connection, are optimized, while different C-structures are tested on the basis of each structure.

1) Inside connection. Connecting the inner protection body with the upper and lower side protection bodies, combining them into a C-shaped structure, and the outer protection body as a separate structure, which allows the distance and thickness of the modules to be varied within certain intervals.

2) Outside connection. Connecting the outer guard body with the side upper and side lower guard bodies, combining them into a C-shaped structure, and the inner guard body as a separate structure, as well as the possibility of varying the distance and thickness of the modules within certain intervals.

3) Surrounding structure. Wrap-around structure is a hollow cylinder, the greater thickness of the protection effect the better, but the cost will increase significantly. Therefore, it is necessary to determine a appropriate thickness to realize the economy and versatility of the protective structure.

3. SIMULATION ANALYSIS AND DISCUSSION

Based on ANSYS Electronics to build a three-dimensional orbit gas pedal and guard model, the peak value of the incoming current is 281.98 kA, the mass of the armature 10 g, and the length of the track test 500 mm, ignoring the sliding wear

TABLE 2. Evaluation function values of some protective materials.

Serial number	Material	Protective efficacy	Stiffness	Reliably	Maneuverability	Cost	Scoring function
Material 1	Aluminum	1	650	2	0.37	76.92	1848.96
Material 2	Iron	300	274	1	0.127	249	1206.4
Material 3	Cast iron	425	1450	1	0.128	200	2935.2
Material 4	Mumetal Permalloy	12000	900	3	0.114	4.35	75523.55
Material 5	Cold-rolled steel	2400	1500	2	0.127	333.33	14167.05
Material 6	Steel1008	2000	330	1	0.127	100	4529.191
Material 7	Stainless steel	1500	2500	1	0.127	100	6350.191
Material 8	High magnetic steel	8500	331	1	0.131	28.57	17459.07
Material 9	Graphene-glass fiber	280	600	3	0.5	800	6422.25

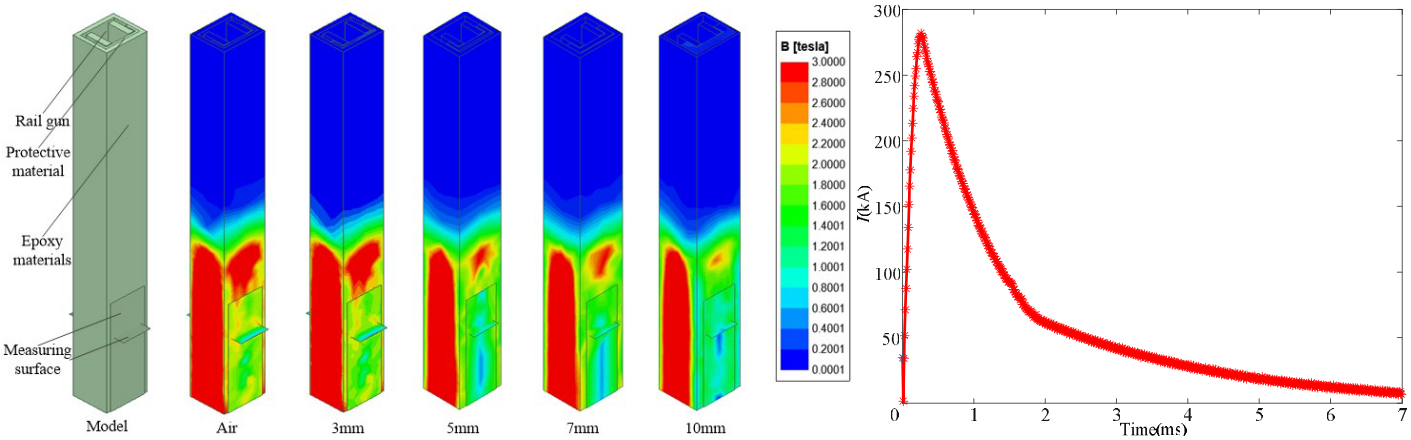

FIGURE 2. Simulation of the structure of the inner connection shield.

in the armature movement process. In the same environment, the input current curves generated by pulse capacitors with the same charging voltage and energy storage exhibit minimal differences.

3.1. Protective Material Selection Evaluation Function Value

The materials and parameters in Table 1 correspond to the calculation of the scores of different factors. In this paper, the applicable environment of the orbital gas pedal is the low altitude land maneuvering type, so the weight of mobility is set to 1.5, the protection effectiveness weight set to 2, the reliability weight 100, and the rest of the weights set to 1. The relative thickness of the protective body in the irrelevant variables is 5 mm; the ambient temperature is 25°C; the average value is taken when the value of the relative permeability parameter is in the interval; the impact resistance and density parameters are in the interval to the highest value; and the values of the evaluation function calculated are shown in Table 2.

Combined with the ordering of the evaluation function values in Table 2, Mumetal Permalloy is selected as the material for the fabrication of the protective body for a single material for the environment of high mobility in low altitude land.

3.2. Inside Connection Guard Structure

The medial connection topology is to connect the medial protection area to the protection area above and below the side in a right angle C-shape, and the critical value of the shielding magnetic field target can be achieved by changing the thickness test. The results of the inner connection protection are shown in Fig. 2.

The simulation results show that the magnetic field strength on the outer surface of the device is above 1 T, and the shielding performance is not perfect. Based on the eddy current field and transient field analysis, it can be seen that the high flux density region is distributed around the radiation sourc; the shieldable area of the material placed on the inner side is small; and the flux density in some areas cannot be centralized to flow to the shielding material.

3.3. Outer Connection Protection Structure

The outer connection topology connects the outer shielding structure to the upper and lower side shielding areas in a right-angled C-shape, placing the shielding material outside the fixed enclosure, which theoretically increases the cost of materials used due to the larger size of the outer connection shielding structure. On the other hand, as the magnetic field attenuates with distance, the need for shielding performance decreases, reducing the cost of materials used. Shielding materials were

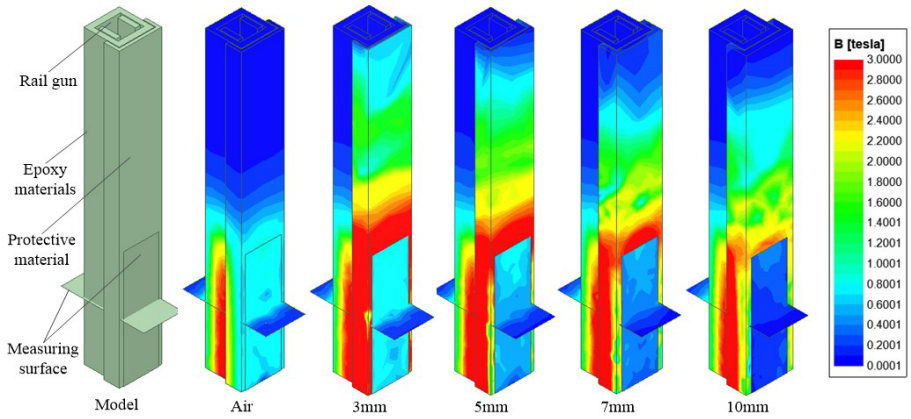

FIGURE 3. Simulation of the structure of the outer connection shield.

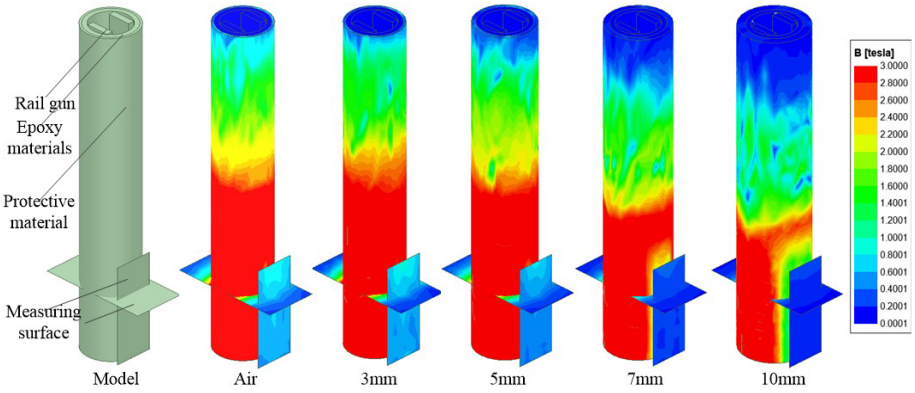

FIGURE 4. Shielding effect of different thicknesses of wrap-around structures.

added to the periphery of the epoxy layer, testing the shielding effect for thicknesses of 3 mm, 5 mm, 7 mm, and 10 mm, respectively.

Simulation results in Figure 3 demonstrate a significant decrease in the magnetic field strength on the measurement surface as the thickness of the outer guard is increased. Specifically, when the thickness reaches 7 mm, the magnetic field strength on the surface of the device decreases to within 0.5 T, with the majority of the area measuring less than 0.3 T. For larger surrounding spaces, a shielding device with a thickness of 5 mm can be utilized. However, it is important to ensure that sensitive components are kept at a distance greater than 5 mm from the surface of the device.

3.4. Wrap-around Protection Structure

In order to increase the fixing strength of the epoxy shell and protection device, the shielding effect of the cylindrical structure is simulated. The basic parameters of the test remained unchanged, and the epoxy layer was used as a fixing device with a thickness of 6 mm. Increase the shielding material in the periphery of the epoxy layer, respectively test the thickness of 3 mm, 5 mm, and 7 mm shielding effect.

The simulation results presented in Figure 4 demonstrate that increasing the thickness of the protective layer to 7 mm effectively controls the magnetic field strength on the measurement surface within 0.5 T, with certain areas even achieving a stability of 0.2 T. Furthermore, a thickness of 10 mm ensures a stable magnetic field strength of 0.2 T on the measuring surface. However, it is important to note that when the distance from the track exceeds 45 mm, the magnetic field strength drops below 0.1 T.

By conducting a comprehensive analysis of the various dimensions of protective materials, this study aims to screen and examine the selection factors that are closely associated with material performance. Subsequently, an applicability evaluation function for protective materials will be developed by assigning different weights and incentive functions to these factors. As shown in Figure 5, it is evident that external protection and ring protection yield better results than the internal protection structure. At a thickness of 10 mm, both external protection and ring protection manage to reduce the magnetic field intensity to less than 0.1 T. The thickness and shielding performance of protective materials of different structures were analyzed, and points were taken at intervals on the centerline of the measurement surface to synthesize a three-dimensional function of thickness-taking position-magnetic field strength.

Both the outer shielding structure and the wrap-around shielding structure in Figure 5 can be approximately 6 mm thick to achieve the protection requirements. Calculating the cost of shielding material for the same 6 mm thickness for both structures yields a volume of 7.98×10^5 mm^3 of shielding material for the wrap-around type and a volume of 6.6×10^5 mm^3

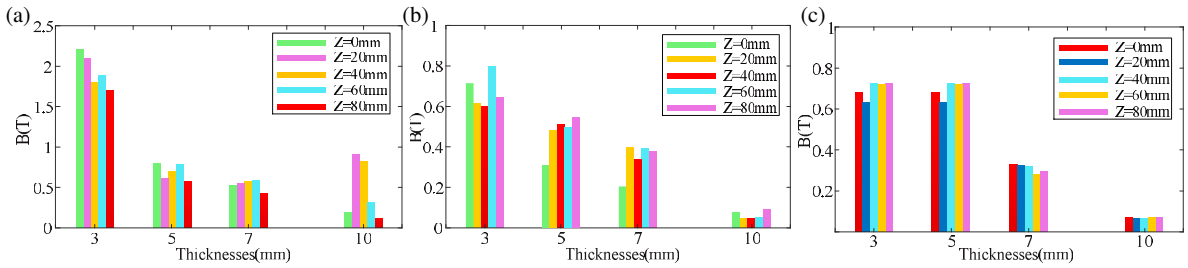

FIGURE 5. Shielding material thickness and magnetic induction after shielding. (a) The thickness of the inner protective structure and the magnetic induction intensity after shielding. (b) Thickness of outer protective structure and magnetic induction intensity after shielding. (c) Thickness of the shielding material of the wrap-around structure and the magnetic induction strength after shielding.

for the outer shielding structure (which needs to be retrofitted on both sides of the track). However, wrap-around installations are more costly and require more workmanship. Therefore, when the model in this paper is applied to an integrated device, a wrap-around shielding structure can be used; when it is applied to an ordinary assembled device or when only one side of the magnetic field needs to be shielded, an outer add-on shielding structure is used.

4. CONCLUSION

This study addresses the issue of excessive radiation generated by the pulsed electromagnetic gas pedal during operation and its interference with the external environment. By integrating the principles of electromagnetism, topology, and material science, this paper proposes a method for designing the material and topology of the radiation source protection body.

The following conclusions are drawn from our research:

1) A multi-factor material selection model is established through principal component analysis by defining selection factors for protective materials and assigning different weights to these factors based on the application environment. Through calculation, Mumetal permalloy is selected as the optimal protective material.

2) A topological model of the shielding body is developed, which identifies six regions where the shielding body can be added. By considering the cost of the shielding material as the target value, different connection methods are explored to obtain three distinct shielding structures: proximal, distal, and encircling. Through simulation analysis, the paper summarizes the relationship between material thickness and shielding effectiveness. In comparison to the traditional material selection method, the model proposed in this paper takes into account additional reference factors such as corrosion resistance and cost-effectiveness.

3) For higher protection requirements, the topology model presented in this paper offers a solution by either increasing the protection area or augmenting the thickness of the protection body. For example, when the need for protection is increased to within 0.05 T, it is only necessary to increase the thickness to 13 mm to satisfy the need. However, the radiation calculation employed ANSYS simulation, although it was noted that the simulation time was lengthy. Moving forward, our future work will focus on reducing computational costs, enhancing simulation speed, and refining the coupling effect of the model.

REFERENCES

[1] Yang, B., *Artillery Firing Technology*, Arms Industry Press, Beijing, 34–67, 1993.

[2] Zhou, Y., X. Lu, and D. Liu, "Exploratory study on the feasibility of several ultra-high-speed projectile launching techniques," *Journal of Ballistics*, Vol. 8, No. 4, 8–12, 1996.

[3] Ang, J. A. and C. H. Konrad, "Hypervelocity projectile design and fabrication," *IEEE Transactions on Magnetics*, Vol. 29, No. 1, 722–728, Jan. 1993.

[4] Sun, B., "Modeling and simulation optimization of three-stage electromagnetic transmitter," Ph.D. dissertation, 2-3, Harbin Institute of Technology, Harbin, 2006.

[5] Lin, Q. and B. Li, "Measurement and numerical simulation of transient magnetic field of electromagnetic railgun," *Journal of Military Engineering*, Vol. 37, No. 10, 1788–1794, 2016.

[6] Kul'ment'eva, O. P. and A. D. Pogrebnyak, "Effect of pulsed plasma and high-current electron beam treatments on the structure and properties of nickel-based coatings," *Journal of Surface Investigation. X-ray, Synchrotron and Neutron Techniques*, Vol. 2, No. 3, 454–473, Jun. 2008.

[7] Zhang, M., "Research on electromagnetic characteristics and anti-interference technology of power supply system during electromagnetic cannon firing process," Ph.D. dissertation, Nanjing University of Science and Technology, 2017.

[8] Zhang, M., N. Shen, and H. Tian, "Research on the shock characteristics of distributed pulse power system during the launching process of electromagnetic railgun," *Journal of Military Engineering*, Vol. 38, No. 5, 2017.

[9] Luo, H. and X. Mei, "Hazards of strong magnetic fields on fuzes of electromagnetic launching munitions and their protection," *Digital Ocean and Underwater Attack and Defense*, Vol. 4, No. 1, 58–62, 2021.

[10] Liao, Q., X. Zhang, H. Li, and N. Shen, "Design and simulation of shielding for strong magnetic field environment where railgun projectiles are located," *Journal of Artillery Launch and Control*, Vol. 37, No. 2, 67–72, 2016.

[11] Li, F., "Research on shielding and utilization of strong magnetic field environment of electromagnetic railgun," Ph.D. dissertation, Nanjing University of Science and Technology, 2017.

[12] Ji, X., F. Sun, R. Bai, and Z. Yang, "Electromagnetic protection method for electromagnetic artillery projectile telemetry device," *Journal of Detection and Control*, Vol. 41, No. 2, 57–62, 2019.

[13] Gao, H., "Research on shielding effectiveness of measurement and control unit of pulsed power source and analysis of internal magnetic field distribution," Ph.D. dissertation, Nanjing University of Science and Technology, 2009.

[14] Schneider, M., R. Schneider, V. Stankevic, S. Balevicius, and N. Zurauskiene, "Highly local measurements of strong transient

magnetic fields during railgun experiments using cmr-based sensors," *IEEE Transactions on Magnetics*, Vol. 43, No. 1, 370–375, Jan. 2007.

[15] Riccardo, C., M. Schneider, and B. Tellini, "The use of electronic components in railgun projectiles," *IEEE Transactions on Magnetics*, Vol. 45, No. 1, 578–583, Jan. 2009.